Geophysical Research Letters

RESEARCH LETTER
10.1029/2018GL078256

Special Section:
Cassini's Final Year: Science Highlights and Discoveries

Discovery of Atmospheric-Wind-Driven Electric Currents in Saturn's Magnetosphere in the Gap Between Saturn and its Rings

K. K. Khurana[1], M. K. Dougherty[2], G. Provan[3], G. J. Hunt[2], M. G. Kivelson[1], S. W. H. Cowley[3], D. J. Southwood[2], and C. T. Russell[1]

[1]Institute of Geophysics and Planetary Physics and Department of Earth, Planetary and Space Sciences, University of California, Los Angeles, CA, USA, [2]Physics Department, The Blackett Laboratory, Imperial College London, London, UK, [3]Department of Physics and Astronomy, University of Leicester, Leicester, UK

Key Points:
- During Cassini's Grand Finale orbits, the spacecraft identified strong but variable field-aligned currents inside Saturn's D ring
- The current is generated when the two ends of a field line are embedded in zonal atmospheric flows that have differing wind speeds
- The wind-generated currents dissipate 2×10^{11}TW of thermal power in the low-latitude thermosphere, similar to the input from the solar EUV flux in this region

Correspondence to:
K. K. Khurana,
kkhurana@igpp.ucla.edu

Citation:
Khurana, K. K., Dougherty, M. K., Provan, G., Hunt, G. J., Kivelson, M. G., Cowley, S. W. H., et al. (2018). Discovery of atmospheric-wind-driven electric currents in Saturn's magnetosphere in the gap between Saturn and its rings. *Geophysical Research Letters*, *45*, 10,068–10,074. https://doi.org/10.1029/2018GL078256

Received 20 APR 2018
Accepted 4 JUL 2018
Published online 3 OCT 2018

Abstract Magnetic field observations obtained by the Cassini spacecraft as it traversed regions inside of Saturn's D ring packed a genuine surprise. The azimuthal component of the magnetic field recorded a consistent positive perturbation with a strength of 15–25 nT near closest approach. The closest approaches were near the equatorial plane of Saturn and were distributed narrowly around local noon and brought the spacecraft to within 2,550 km of Saturn's cloud tops. Modeling of this perturbation shows that it is not of internal origin but is produced by external currents that couple the low-latitude northern ionosphere to the low-latitude southern ionosphere. The azimuthal perturbations diminish at higher latitudes on field lines that connect to Saturn's icy rings. The sense of the current system suggests that the southern feet of the field lines in the ionosphere leads their northern counterparts. We show that the observed field perturbations are consistent with a field-aligned current whose strength is ~1 MA/radian, that is, comparable in strength to the planetary-period-oscillation-related current systems observed in the auroral zone. We show that the Lorentz force in the ionosphere extracts momentum from the faster moving low-latitude zonal belt and delivers it to the northern ionosphere. We further show that the electric current is generated when the two ends of a field line are embedded in zonal flows with differing wind speeds in the low-latitude thermosphere. The wind-generated currents dissipate 2×10^{11}W of thermal power, similar to the input from the solar extreme ultraviolet flux in this region.

Plain Language Summary The Cassini spacecraft observed strong electric currents aligned along Saturn's magnetic field as it traversed regions inside Saturn's D ring. Modeling and analysis of these currents show that their origin lies in the neutral winds observed in the upper atmosphere of Saturn. The wind-generated currents dissipate a modest amount of energy, which is roughly equal to that coming from solar extreme ultraviolet rays.

1. Introduction

Saturn, a gas giant with an equatorial radius of 60,268 km is the second largest planet of the solar system. Saturn's large magnetosphere (dayside magnetopause distance = 20 R_S) is maintained by its strong axially symmetric magnetic field (equatorial strength = 0.2 Gauss) and a plasma population derived from its satellite Enceladus (Gombosi et al., 2009). The magnetosphere obtains most of its energy from Saturn's rotation and is known to display diurnal periodicities in many field and plasma parameters measured in the magnetosphere (Carbary & Mitchell, 2013; Gurnett et al., 2007).

During its Grand Finale phase, Cassini completed 22 highly inclined orbits that brought it repeatedly to within 1,290–3,300 km from the 1 bar surface of Saturn during the closest approaches (CAs). All of the CAs were inside of the innermost ring of Saturn (the D ring) and provided valuable in situ observations near the thermospheric/ionospheric region of Saturn (Wahlund et al., 2018). The Grand Finale orbits were also ideal for characterizing the internal field of Saturn and the low- and high-latitude current systems that couple to Saturn's ionosphere (Dougherty et al., 2018). In this work, we report on the discovery of low-latitude, strong field-aligned currents that are generated by shears in Saturn's upper atmospheric winds.

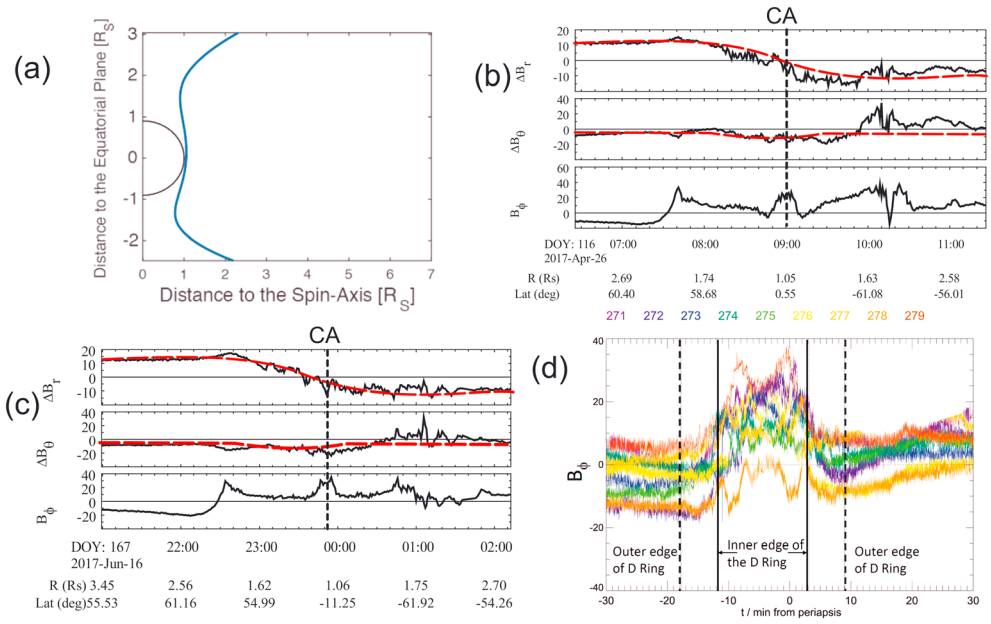

Figure 1. (a) Cassini's trajectory in a cylindrical coordinate system during Rev. 271–279. (b) Perturbation magnetic field (observations-model) from Rev. 271 in spherical coordinate system (black lines). Also shown in broken red lines are the field contributions from Saturn's magnetodisc, which were obtained from the model of Giampieri and Dougherty (2004). (c) As in (b) for Rev. 279. (d) One-hour plots of the azimuthal component of the magnetic field (in nanotesla) from the first nine Grand Finale orbits centered around the CA. The solid and broken vertical lines mark the inner and outer edges of the D ring. Colors indicate orbit numbers as shown above the plot.

2. Spacecraft Trajectory and Observations

The highly inclined Grand Finale orbits (also called proximal orbits, orbital inclination ~ 63°) repeatedly dove the spacecraft through the gap between Saturn's innermost ring and its upper atmosphere (Edgington & Spilker, 2016). The Cassini magnetometer measured and characterized Saturn's dynamo-generated magnetic field to degree 12 during these passes (Dougherty et al., 2018). The measured magnetic field strength exceeded 20,000 nT near the CA. Because in such a strong magnetic field, even an error of 0.1 ^{O} in the knowledge of the orientation of the magnetometer sensor produces an error of the order of 30 nT in the vector measurements, specially designed spacecraft spin maneuvers were performed (Dougherty et al., 2018) during four of the flybys to achieve the absolute orientation of the magnetometer sensors relative to the spacecraft with the same precision as Cassini's Attitude and Articulation Control Subsystem (~0.01°; Lee & Hanover, 2005). The fully calibrated data have errors $<$4 nT (i.e., below the digitization step of 5.4 nT in the high range mode). So far, the first nine Grand Finale orbits (orbits 271–279) have been calibrated using this technique and we shall use data only from these nine flybys.

Figure 1a shows the trajectory of Cassini during these flybys in a cylindrical coordinate system whose z axis is aligned with Saturn's spin axis while the ρ axis points in the cylindrical radial direction. The CAs occurred just south of the equatorial plane of Saturn, and during these nine orbits their CA altitudes varied between 2,500 and 3,300 km from the 1 bar surface. Figure 1b shows approximately 5 hr of magnetic field data (black traces) in the KRTP (spherical) coordinate system centered on the CA from orbit 271. Also plotted in dashed red lines is the expected magnetodisc field computed from the model of Giampieri and Dougherty (2004) by using the following magnetodisc parameters (a,b,D,$\mu_0 I$) = (6.5 R_S, 25 R_S, 2.5 R_S, 48.5 nT). The spacecraft traveled north to south covering a latitudinal range of ~60° to ~ −60° during this time and remained within a radial distance of ~3 R_S from Saturn. In order to focus on Saturn's weak external field, we have subtracted the degree 12 internal field model presented by Dougherty et al. (2018) from the observations. Because Saturn's internal field is highly axisymmetric, the contribution from the model field to the B_ϕ component is zero.

Several remarkable features are seen in the residual field. First, the perturbation field in the r and θ directions (ΔB_r and ΔB_θ) is clearly dominated by the field generated by Saturn's magnetodisc. The azimuthally drifting

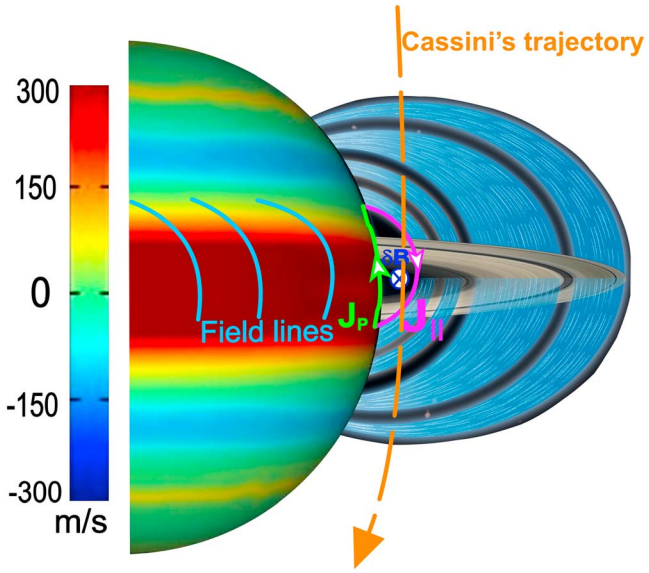

Figure 2. Generation of Pedersen (green line) and field-aligned (magenta) currents in Saturn's ionosphere/magnetosphere system from wind-velocity differential between the two ends of a field line. Color shading on Saturn's surface represents zonal wind velocities.

particles of the magnetodisc produce a distinct depression in the observed ΔB_θ near the CA and a positive ΔB_r when the spacecraft is above the equatorial plane and a negative ΔB_r when the spacecraft is below the equatorial plane. Next, at high latitudes, all three components of the magnetic field (especially B_ϕ) show perturbations caused by field-aligned current systems associated with the planetary period oscillation (PPO) and plasma subcorotation that link the auroral region of the ionosphere to the magnetosphere (Hunt et al., 2014, 2015). Finally, a surprisingly large positive perturbation exceeding 20 nT is seen in the azimuthal component near the equatorial plane of Saturn. The perturbation decays in amplitude to almost zero during the time when the spacecraft is located on field lines that connect to the rings of Saturn. Figure 1c shows the perturbation field observed during the 279 periapsis pass in the same format as Figure 1b. Once again, the effects of the magnetodisc ring current are apparent in ΔB_r and ΔB_θ components. The perturbations associated with the subcorotation and PPO current system are also observed in all three components (though clearly different in phase and amplitude from pass 271 because of its dependence on rotation phase). Again, a central positive B_ϕ peak of slightly stronger strength of ~25 nT is observed near the equatorial plane during this flyby. In both of these observational plots (Figures 1b and 1c), the central peak in B_ϕ is not accompanied by perturbations in ΔB_r and ΔB_θ, suggesting that the signal is rotational in nature (B_r and B_θ are the main components of the magnetic field near the equator). The positive sign of the B_ϕ perturbation indicates that the southern ends of the field lines are leading their northern ends in this region.

In order to further understand the nature of this low-latitude perturbation, we have plotted the B_ϕ component of the field over a period of ±30 min around the CA from all nine passes in Figure 1d. It can be seen that even though the central perturbation in B_ϕ is variable from pass to pass, a consistent positive B_ϕ perturbation is present during all of the passes with an average perturbation field of 15–20 nT. It is can be seen that some of the variability to the central peak arises from a changing contribution of PPO origin, which changes the baseline of the central peak from pass to pass. However, some of the variability of this feature is also due to other causes (it has a temporal nature) as seen in the changing shape and strength of the central peak. The B_ϕ perturbation region is terminated on both sides by the inner edge of the D ring suggesting that Saturn's icy rings act as barriers to field-aligned currents flowing on these field lines. As the spacecraft was traveling toward Saturn when it was in the northern hemisphere, a sharp positive slope in B_ϕ indicates that the spacecraft crossed a sheet of southward field-aligned current. Similarly, a negative slope in B_ϕ on field lines in the southern hemisphere when the spacecraft was traveling away from Saturn indicates that the spacecraft again crossed the same sheet of southward directed field-aligned current. As no oppositely directed (i.e., northward) currents were observed on these field lines, we conclude that the closure currents must be flowing on field lines that are planetward of Cassini's location.

3. The Origin of Field-Aligned Currents

A clue to the origin of these field-aligned currents emerges when we examine their closure geometry (Figure 2). The consistent positive B_ϕ perturbation observed by Cassini near the equatorial plane suggests that the spacecraft passed in between two shells of oppositely directed currents. The outer shell was crossed by Cassini twice and is composed of field-aligned currents that are flowing in the southward direction. The inner shell was not crossed by Cassini, and therefore, its location is uncertain. It carries return current that could be flowing either along field lines or through the ionosphere of Saturn. Current continuity requires that these two current shells be connected with each other through ionospheric currents flowing in the $-\theta$ direction (northward) in both ionospheric hemispheres (see Figure 2 where we have assumed closure through Saturn's ionosphere). As the radial component of Saturn's magnetic field is directed radially inward in the southern hemisphere and outward in the northern hemisphere, the azimuthal component of the Lorentz force, $(\mathbf{J} \times \mathbf{B})_\phi = J_r B_\theta$ associated with the Pedersen currents is directed in the $-\phi$ in the southern segment of the ionosphere and in the $+\phi$ direction in the northern segment. Thus, the field lines in the

inner magnetosphere are extracting momentum from the southern ionosphere and passing it on to the northern ionosphere. For interhemispheric transfer of momentum to occur, the southern ionospheric annulus connected to these field lines must have surplus azimuthal momentum compared to the corresponding northern ionospheric annulus. This momentum transfer picture also explains why the southern ends of the field lines appear to lead their northern counterparts producing a positive B_ϕ perturbation (blue field lines in Figure 2).

The next obvious question is why is this momentum exchange occurring between the two ionospheric segments? The answer can be found in the wind patterns observed in the atmospheric layers below the ionosphere and the fact that Saturn's magnetic dipole is displaced northward by ~0.047 R_S (Dougherty et al., 2018). It is well known that winds in Saturn's troposphere have a zonal structure (Sánchez-Lavega, 2005) with the fastest winds (as much as 430 m/s above the average value) occurring in an equatorial band with a latitudinal half-width of ~20° (depicted by the red equatorial band in Figure 2). There is good evidence that the equatorial high-speed band extends into the stratosphere (Fletcher et al., 2012) and also into the mesosphere (Hubbard et al., 1997). We shall assume that the zonal structure of the neutral winds extends further up into the thermosphere where direct measurements do not exist. Next, because of the northward displacement of the magnetic dipole, the field lines that cross the inner edge of the D ring map to a latitude of 25.1° in the northern ionosphere (outside of the fast equatorial jet) but to a latitude of −16.3° in the south (well within the equatorial jet). Thus, the two ends of the footprints of these field lines experience an azimuthal velocity difference of ~300 m/s, with the southern ends that are embedded in the equatorial belt experiencing faster neutral winds. Ions on the same field lines, however, must maintain a constant velocity everywhere because of their extreme field-aligned mobility. We shall assume that the ions adopt a velocity that is an arithmetic average between the velocities of the neutrals in the ionosphere at the two ends of the field lines. Thus, the ions on these field lines are moving slower than the neutrals in the (equatorial-belt) southern ionosphere but are moving faster than the neutrals in the northern ionosphere (which are outside of the equatorial belt). In the rest frame of the ionospheric neutrals, ions experience a meridional electric field, E, given by (see, e.g., Huang & Hill, 1989)

$$E = (V_i - V_n)2B_S \cos\theta = \pm\Delta V_{\text{zonal}} B_S \cos\theta \tag{1}$$

Here V_i and V_n are the velocities of ions and neutrals respectively, B_S is the surface magnetic field of Saturn at its equator, θ is the colatitude, and ΔV_{zonal} is the velocity difference between the zonal winds at the southern and northern ionospheric footprints. In equation (1), the positive sign applies for the northern latitudes and the negative sign applies for the southern latitudes.

At both ends of the field lines in the ionosphere, the electric field drives a meridional (northward) Pedersen current, J_P, given by

$$J_P = \pm\sigma\Delta V_{\text{zonal}}\ B_S\ \cos\theta \tag{2}$$

where σ is the conductivity of the ionosphere. This equation can be integrated over the thickness of the ionosphere and in longitude to get the Pedersen current flowing per azimuthal radian in the ionosphere:

$$I_P = \pm\Sigma R_S \Delta V_{\text{zonal}} B_S \cos\theta \tag{3}$$

where Σ is the height-integrated Pedersen conductivity of the ionosphere.

These Pedersen currents couple the plasma with the neutrals of the ionosphere at both ends of the field lines. Thus, a picture emerges of ionospheric magnetobraking, where the field lines mapping into the equatorial zonal belt are continually slowing the neutrals (by coupling them with the slower ions) and are transferring the momentum to the neutrals of the slower northward zonal belt. It should be clear that unless the momentum of the neutrals in the ionosphere is continually replenished by vertical transfer of angular momentum from below (the mesosphere), the two adjacent zonal belts in the thermosphere would equilibrate to a common average flow speed and the Pedersen and associated field-aligned currents would cease to flow. The fact that Cassini observed field-aligned currents in this region during every flyby during the Grand Finale orbits suggests that differences in the thermospheric zonal wind velocities are being maintained by enhanced transfer of angular momentum in the equatorial belt through eddy diffusion (Sandel, 1982),

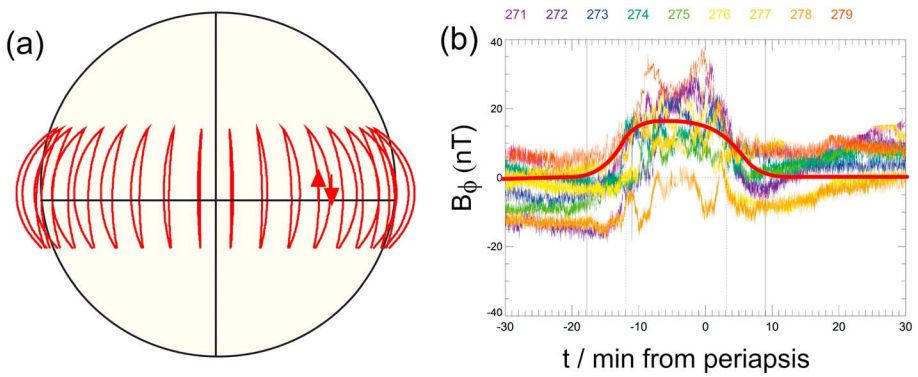

Figure 3. (a) Computational wire mesh model used in Biot-Savart field modeling. The electric current travels from north to south on magnetic field lines but returns from south to north in the ionosphere. (b) Best fit model (thick red line) superimposed on the observed azimuthal component of the magnetic field from the first nine Grand Finale orbits (color coded).

meridional advection (Smith et al., 2007), and other atmospheric wave processes such as gravity waves (Müller-Wodarg et al., 2006).

The Pedersen currents also heat the thermosphere/ionosphere region through Joule dissipation, given by J_P^2/σ. Equations (2) and (3) show that the Pedersen currents generated by this coupling process increase with latitude and vanish near the magnetic equator. Two processes contribute to the reduction of the current near the equator, the reduction in the strength of the radial component of the magnetic field and a reduction in ΔV_{zonal} from the fact that both ends of the very short field lines near the equator are embedded in essentially the same flow.

4. Biot-Savart Modeling of Wind-Generated Magnetic Fields

In order to quantitatively interpret the strengths of the field-aligned currents generating the observed magnetic field perturbations, we have modeled the observations using a Biot-Savart computational model. The computational wire mesh model (see Figure 3a) consists of two sets of current-carrying filaments. The first set of 36 filaments carries southward field-aligned current and follows the field lines of the C6 model that just touch the inner edge of the D ring in the equatorial plane and are separated by 10° in azimuth. The second set of filaments carries return current (northward) through the surface of Saturn (at ionospheric heights) and has the same latitudinal extent as the first set of filaments. Each of the 72 filaments is further composed of 100 straight segments and all carry the same amount of electric current whose value was optimized to obtain the best fit shown in Figure 3b. This choice of the return-current geometry (i.e., closure along the surface of Saturn) is roughly consistent with equation (3), which stipulates that the maximum Pedersen current should be observed at the highest latitudes and its strength should fall to zero at the equator. Indeed, in our model, the largest Pedersen currents in the ionosphere are at latitudes that map to the inner edge of the D ring. Even though the strength of the current remains constant in the ionosphere, it gradually becomes more field aligned with decreasing latitude.

The magnetic field from each of the segments was calculated from Biot-Savart equation generalized for a segment of arbitrary length (Khurana et al., 2007):

$$\mathbf{B} = \int_{\theta_1}^{\theta_2} \frac{\mu_0 I}{4\pi} \frac{\mathbf{dl}\times\mathbf{R}}{R^3}\hat{\varphi} = \frac{\mu_0 I}{4\pi\rho}\,(\sin\theta_2 - \sin\theta_1)\hat{\varphi} \tag{4}$$

where **dl** is an infinitesimal segment of the finite length segment over which the integration is performed, **R** is the vector radial distance of the infinitesimal segment from the point of measurement, and θ_2 and θ_1 are the angles subtended by the two ends of the finite length segment to the normal to the segment and the observer. *I* is the strength of the current (in Amperes) carried by each segment.

The best fit model (thick red line on Figure 3b) was obtained for a current strength of 0.2 MA in each filament. The integrated total current strength is therefore 7.2 MA or 1.15 MA/radian in each of the shells. Substituting

this value of current in equation (3), we find that $\Sigma = 8.89$ S for a zonal wind shear $\Delta V_{zonal} = 300$ m/s. This value of height-integrated Pedersen conductivity is consistent with those derived from Cassini's observations of the electrons and neutrals in the ionosphere (Kliore et al., 2009; Moore et al., 2010).

5. Heating of the Thermosphere by Joule Dissipation

As alluded to in section 3, Pedersen currents flowing in the ionosphere create heat through Joule dissipation. The total heat generated per second in the low-latitude ionosphere is given by

$$\dot{Q}(\text{Watts}) = \iiint_{r,\theta\varphi} R_S^2 \sigma E^2 \sin\theta d\,\theta d\,\varphi = \frac{4}{3}\pi R_S^2 \Sigma \Delta V^2 B_s^2 \cos^3 70^o = 2.2\times 10^{11}\text{W}$$

where we have assumed that the neutral wind velocity shear is 300 m/s and heating is generated in a latitudinal band of ±20°. When divided by the surface area of the low-latitude ionosphere, this heat output is equivalent to 0.014 mW/m^2, an energy input similar to that from the solar extreme ultraviolet flux into the ionosphere (Galand et al., 2011; Müller-Wodarg et al., 2006). This is a remarkably large addition to the energy budget of the ionosphere. However, the heat addition is not sufficient to explain the very high temperatures observed in Saturn's thermosphere and solve the "thermospheric energy crisis" problem observed on outer planets (Müller-Wodarg et al., 2006; Yelle & Miller, 2004).

6. Conclusions

We have analyzed field-aligned currents that were observed near Saturn's equator inside of the D ring of Saturn and show that the currents are generated by shears in the zonal winds of Saturn's upper atmosphere. The total strength of the observed global current system is ~7 MA, and it dissipates close to 2×10^{11}TW of thermal power in Saturn's low-latitude thermosphere. The presence of these currents provides the first conclusive evidence that the zonal wind flows seen in the troposphere extend high into the thermosphere. The intrinsic variability of the signature from pass to pass (i.e., non-PPO-related changes in the amplitude of B_ϕ) could be related to the variability of the Pedersen conductivity of the ionosphere reported by Wahlund et al. (2018). We would like to point out the close analogy of the heating process discussed in this work with that of heating of the solar corona, where according to one of the leading mechanisms, the mechanical energy associated with the shuffling of the footprints of magnetic field lines in the photosphere ultimately leads to heating of the plasma in the corona.

Acknowledgments
There are no real or perceived financial conflicts of interests for any author. The data used in this work are readily available from the Planetary Data System.

References

Carbary, J. F., & Mitchell, D. G. (2013). Periodicities in Saturn's magnetosphere. *Reviews of Geophysics*, *51*, 1–30. https://doi.org/10.1002/rog.20006

Dougherty, M. K., Cao, H., Khurana, K. K., Hunt, G. J., Provan, G., Kellock, S., et al. (2018). Saturn's magnetic field revealed by Cassini Grand Finale. *Science*. https://doi.org/10.1126/science.aat5434

Edgington, S. G., & Spilker, L. J. (2016). Cassini's Grand Finale. *Nature Geoscience*, *9*(7), 472–473. https://doi.org/10.1038/ngeo2753

Fletcher, L. N., Hesman, B. E., Achterberg, R. K., Irwin, P. G. J., Bjoraker, G., Gorius, N., et al. (2012). The origin and evolution of Saturn's 2011–2012 stratospheric vorte. *Icarus*, *221*, 560–586. https://doi.org/10.1016/j.icarus.2012.08.024

Galand, M., Moore, L., Mueller-Wodarg, I., Mendillo, M., & Miller, S. (2011). Response of Saturn's auroral ionosphere to electron precipitation: Electron density, electron temperature, and electrical conductivity. *Journal of Geophysical Research*, *116*, A09306. https://doi.org/10.1029/2010JA016412

Giampieri, G., & Dougherty, M. K. (2004). Modelling of the ring current in Saturn's magnetosphere. *Annales Geophysicae*, *22*(2), 653–659. https://doi.org/10.5194/angeo-22-653-2004

Gombosi, T. I., Armstrong, T. P., Arridge, C. S., Khurana, K. K., Krimigis, S. M., Krupp, N., et al. (2009). Saturn's magnetospheric configuration. In *Saturn from Cassini-Huygens* (pp. 203–255). Netherlands: Springer. https://doi.org/10.1007/978-1-4020-9217-6_9

Gurnett, D. A., Persoon, A. M., Kurth, W. S., Groene, J. B., Averkamp, T. F., Dougherty, M. K., & Southwood, D. J. (2007). The variable rotation period of the inner region of Saturn's plasma disk. *Science*, *316*(5823), 442–445. https://doi.org/10.1126/science.1138562

Huang, T. S., & Hill, T. W. (1989). Corotation lag of the jovian atmosphere, ionosphere and magnetosphere. *Journal of Geophysical Research*, *94*, 3761–3765.

Hubbard, W. B., Porco, C. C., Hunten, D. M., Rieke, G. H., Rieke, M. J., McCarthy, D. W., et al. (1997). Structure of Saturn's mesosphere from the 28 Sgr occultations. *Icarus*, *130*(2), 404–425. https://doi.org/10.1006/icar.1997.5839

Hunt, G. J., Cowley, S. W. H., Provan, G., Bunce, E. J., Alexeev, I. I., Belenkaya, E. S., et al. (2014). Field-aligned currents in Saturn's southern nightside magnetosphere: Subcorotation and planetary period oscillation components. *Journal of Geophysical Research: Space Physics*, *119*, 9847–9899. https://doi.org/10.1002/2014JA020506

Hunt, G. J., Cowley, S. W. H., Provan, G., Bunce, E. J., Alexeev, I. I., Belenkaya, E. S., et al. (2015). Field-aligned currents in Saturn's northern nightside magnetosphere: Evidence for interhemispheric current flow associated with planetary period oscillations. *Journal of Geophysical Research: Space Physics*, *120*, 7552–7584. https://doi.org/10.1002/2015JA021454

Khurana, K. K., Dougherty, M. K., Russell, C. T., & Leisner, J. S. (2007). Mass loading of Saturn's magnetosphere near Enceladus. *Journal of Geophysical Research*, *112*, A08203. https://doi.org/10.1029/2006JA012110

Kliore, A. J., Nagy, A. F., Marouf, E. A., Anabtawi, A., Barbinis, E., Fleischman, D. U., & Kahan, D. S. (2009). Midlatitude and high-latitude electron density profiles in the ionosphere of Saturn obtained by Cassini radio occultation observations. *Journal of Geophysical Research*, *114*, A04315. https://doi.org/10.1029/2008JA013900

Lee, A. Y., & Hanover, G. (2005). Cassini spacecraft attitude control flight performance. In *Proceedings of the AIAA Guidance, Navigation, and Control Conference* (pp. 8–74). New York: Am. Inst. of Aeronaut. and Astron aut.

Moore, L., Mueller-Wodarg, I., Galand, M., Kliore, A., & Mendillo, M. (2010). Latitudinal variations in Saturn's ionosphere: Cassini measurements and model comparisons. *Journal of Geophysical Research*, *115*, A11317. https://doi.org/10.1029/2010JA015692

Müller-Wodarg, I. C. F., Mendillo, M., Yelle, R. V., & Aylward, A. D. (2006). A global circulation model of Saturn's thermosphere. *Icarus*, *180*(1), 147–160. https://doi.org/10.1016/j.icarus.2005.09.002

Sánchez-Lavega, A. (2005). How long is the day on Saturn. *Science*, *307*(5713), 1223–1224. https://doi.org/10.1126/science.1104956

Sandel, B. R. (1982). Eddy diffusion at Saturn's homopause. *Geophysical Research Letters*, *9*(9), 1077–1080. https://doi.org/10.1029/GL009i009p01077

Smith, C. G. A., Aylward, A. D., Millward, G. H., Miller, S., & Moore, L. E. (2007). An unexpected cooling effect in Saturn's upper atmosphere. *Nature*, *445*(7126), 399–401. https://doi.org/10.1038/nature05518

Wahlund, J.-E., Morooka, M. W., Hadid, L. Z., Persoon, A. M., Farrell, W. M., Gurnett, D. A., et al. (2018). In situ measurements of Saturn's ionosphere show it is dynamic and interacts with the rings. *Science*, *359*(6371), 66–68. https://doi.org/10.1126/science.aao4134

Yelle, R. V., & Miller, S. (2004). Jupiter's thermosphere and ionosphere. In F. Bagenal, W. McKinnon, & T. Dowling (Eds.), *Jupiter: Planet Satellites and Magnetosphere* (pp. 185–218). Cambridge: Cambridge University Press.